Letter

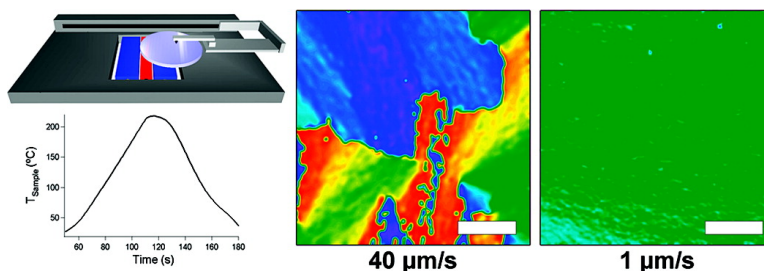# Orientational Order in Block Copolymer Films Zone Annealed below the Order−Disorder Transition Temperature

Brian C. Berry, August W. Bosse, Jack F. Douglas, Ronald L. Jones, and Alamgir Karim

40 µm/s   1 µm/s

More About This Article

Additional resources and features associated with this article are available within the HTML version:

- Supporting Information
- Links to the 5 articles that cite this article, as of the time of this article download
- Access to high resolution figures
- Links to articles and content related to this article
- Copyright permission to reproduce figures and/or text from this article

View the Full Text HTML

ACS Publications
High quality. High impact.

Orientational Order in Block Copolymer Films Zone Annealed below the Order–Disorder Transition Temperature

Brian C. Berry, August W. Bosse, Jack F. Douglas, Ronald L. Jones,* and Alamgir Karim

Polymers Division, National Institute of Standards and Technology, Gaithersburg, Maryland 20899-8541

ABSTRACT

We report measurements of rapid ordering and preferential alignment in block copolymer films zone annealed below the order–disorder transition temperature. The orientational correlation lengths measured after approximately 5 h above the glass-transition temperature (≈ 2 μm) were an order of magnitude greater than that obtained under equivalent static annealing. The ability to rapidly process polymers with inaccessible order–disorder transition temperatures suggests zone annealing as a route toward more robust nanomanufacturing methods based on block copolymer self-assembly.

The self-organization of block copolymer (BCP) films into periodic morphologies such as dense arrays of lines and posts with line widths of (5–50) nm is considered a potential solution to the patterning of dense, high aspect ratio patterns for next generation microelectronics and data storage.[1–4] The critical challenge facing block copolymer self-assembly as a nanofabrication method is the mitigation of defects. Many groups have focused on improving long-range order through a variety of methods including solvent annealing,[5,6] electric fields,[7–13] and thermal annealing of films. Although thermal annealing is the most broadly applicable of the techniques, a significant number of defects persist even after days of uniform annealing. Much work, therefore, has focused on the combination of thermal annealing with top-down approaches such as topographical[14–17] and chemical patterning[18,19] to enhance long-range order and shorten annealing times. "Zone annealing" or "zone refinement" techniques have long been utilized to produce high-purity metals and semiconductors, and the application of this methodology to modify the defect structure of block copolymer materials is thus natural from a practical standpoint of improving long-range order. We investigate long-range orientational order in block copolymer films subjected to a new processing platform based on zone annealing *below* the order–disorder transition temperature.

Traditional zone annealing involves a localized melting followed by recrystallization as the material is moved at a constant velocity (V) over a heated region having a thermal gradient (G) with a fixed slope. In this method, crystallization occurs at a front separating the hot and cold regions. The fact that all growth occurs at this planar front can result in oriented crystals with lower defect densities. This technique has also been shown to successfully control crystal size and orientation in many organic systems.[20–22] Hashimoto and co-workers[23–25] first applied zone annealing to BCP systems to create "defect free" samples with long-range order, and Register and co-workers further explored a novel variation of this method involving an oscillating temperature gradient.[26] Both studies demonstrated that significant improvement in the long-range order can be achieved when the sample is zone annealed above the order–disorder transition temperature, a process we refer to as hot zone annealing (HZA). However, the order–disorder transition temperature (T_{ODT}) is not always accessible for many high-molecular-mass BCPs, including the technologically attractive poly(styrene-*b*-methylmethacrylate) (PS-PMMA). In addition, for cylinder forming BCPs, the cylinder orientation was not correlated with the annealing direction.[26] In this study, we have applied zone annealing to cylinder-forming block copolymer films (PS-PMMA) for which the glass transitions of both component polymers is relatively high ($T_g \approx 100$ °C). Our results indicate that processing these films with "cold zone annealing" (CZA), defined by a sample temperature range, $T_g < T_{Hot} \ll T_{ODT}$, produces preferential alignment of the cylinders as well as a significant improvement in the coarsening of the BCP, leading to relatively long orientational correlation lengths after short annealing times. An exceptional advantage of this technique from an industrial standpoint is the ease

---

* Corresponding author. E-mail: ronald.jones@nist.gov.
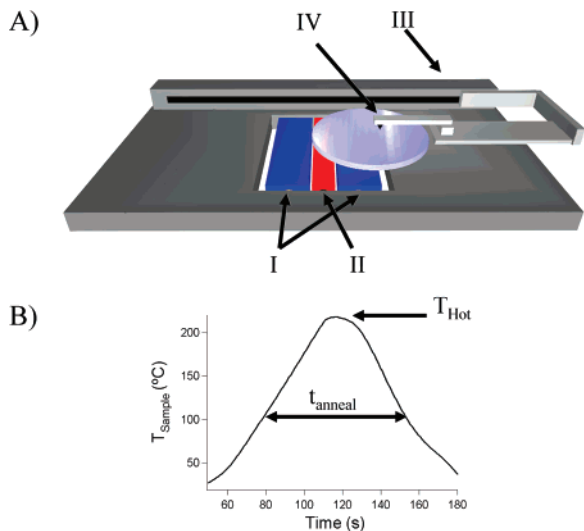
Figure 1. (A) Schematic of the cold zone annealing system. The temperature gradient is established using two temperature controlled cold blocks (I) on each side of a temperature controlled hot block (II). As the sample is pushed across the gradient with a translational motor (III), the temperature profile of the sample at a given point is recorded using a spring loaded thermocouple (IV). (B) Actual temperature profile recorded for a sample zone annealed at a velocity of 200 μm/s. The maximum sample temperature (T_{Hot}), and the time over which the sample is above the apparent T_g (t_{anneal}) are noted.

with which it could be adapted to rapid roll-to-roll processing with virtually no limitations to sample dimensions.

A schematic of the CZA instrument is shown in Figure 1a. The temperature gradient is established using two cold blocks (I) placed on each side of a temperature controlled hot block (II). The blocks are laterally separated from each other by a 1 mm air gap. Each of the cold blocks are constructed from a 25 mm × 100 mm aluminum block with a 6.35 mm hole through the center. Cold water from a programmable circulating water bath is passed through the blocks to maintain constant temperature. The hot block is constructed from a 12 mm × 100 mm aluminum block containing a Watlow heating cartridge (250 W) controlled by an Omega controller (CNi8).[27] Rectangular samples, which are cut from standard 100 mm Si wafers, with widths ranging from 10 to 100 mm and lengths ranging from 40 to 150 mm are translated across the cold and hot blocks at varying velocities using a push arm connected to an LEP Bioprecision microscope stage (model 99S021) (III). The stage velocity and total distance traveled is controlled using a LEP Mac5000 controller interfaced with LabView. To ensure adequate thermal contact of the sample with the cold and hot blocks, the top surface of the cold and hot blocks are coated with a thermally conductive paste (Dow Corning 340 silicone heat sink compound). The temperature profile at a given point is recorded during translation of the sample using a spring-loaded thermocouple (IV). Figure 1b is a recorded temperature profile for a sample zone annealed at a velocity of 200 μm/s. The entire assembly is enclosed in a polycarbonate glove box chamber with nitrogen circulated in it. We note that, in the present setup, there is no temperature control across the top face of the sample wafer,

so a vertical thermal gradient is expected to be present in addition to the lateral thermal gradient from the zone annealing assembly.

For this study, thin films ($t \approx 168$ nm, or 6.5 L_o where t is the film thickness and L_o is the lattice spacing) of asymmetric poly(styrene-b-methyl methacrylate) (molar mass = 47.7 kg/mol, volume fraction of polystyrene = 0.74) (Polymer Source, Inc.) were spun-cast from a 4% toluene solution onto O_2 plasma-cleaned Si wafers. The as-prepared films were pushed at varying velocities ($V = 1-500$ μm/s) through a temperature gradient such that the maximum (T_{Hot}) and minimum (T_{Cold}) sample temperatures were 210 and 40 °C, respectively. In this study, the slope of the linear region of the temperature profile was kept constant at 17 °C/mm. Atomic force microscopy (AFM) phase images were then obtained using an Asylum MFP3D atomic force microscope in tapping mode. Images were collected near the thermocouple location because the exact thermal history of that location was known.

To quantify the orientational order at the surface for these samples, AFM phase images were analyzed using the methods described by Harrison et al.[28−30] To determine the cylinder orientation, the local gradient in intensity for each point in the AFM phase image was calculated.[29] The local gradient was then averaged over an area equal to that of the square of the domain size to account for regions where the gradient magnitude was small and not well defined (e.g., cylinder centers). The angle of this gradient vector in reference to the horizontal axis of the image was defined as the cylinder orientation angle (θ). The color bar below the orientation maps correlates color with cylinder orientation. These orientation maps provide a straightforward method for visualizing BCP grains. The vectors describing local orientation are also used to construct an order parameter field for 2-fold symmetry, defined as $\psi(\mathbf{r}) = e^{2i\theta(\mathbf{r})}$, where θ is the cylinder orientation as defined above and $\mathbf{r}$ is the position vector. The orientational correlation function is then calculated using $g(\mathbf{r}) = \langle \psi(0)\psi(\mathbf{r}) \rangle$, where the angular brackets indicate averaging over all angles for a given distance. An estimated orientational correlation length (ξ) of a sample can then be obtained by fitting $g(\mathbf{r})$ to an exponential $e^{-r/\xi}$.

As shown in Figure 2, the defect density of these samples decreases significantly with decreasing velocity. The defect density is particularly small for $V = 1$ μm/s, where few defects arise in the 2 μm × 2 μm area selected from a 5 μm × 5 μm scan. In addition to the AFM phase images, false color maps of the cylinder orientation angle are shown. Although Figure 2d shows near-perfect order across the image area, larger area images provide a more comprehensive picture of grain sizes and orientational order. Figure 3a contains the false color cylinder orientation map calculated from a 10 μm × 10 μm AFM phase image of a sample zone annealed at 1 μm/s. Large grains can be observed across the 100 μm² area. Figure 3b is an enlarged image showing the microstructure within the 2 μm × 2 μm area shown in Figure 3a. The large grain size and low defect concentration observed with CZA is remarkable when one considers that previous studies[31] on monolayer films ($t \approx 1.5$ L_o) of
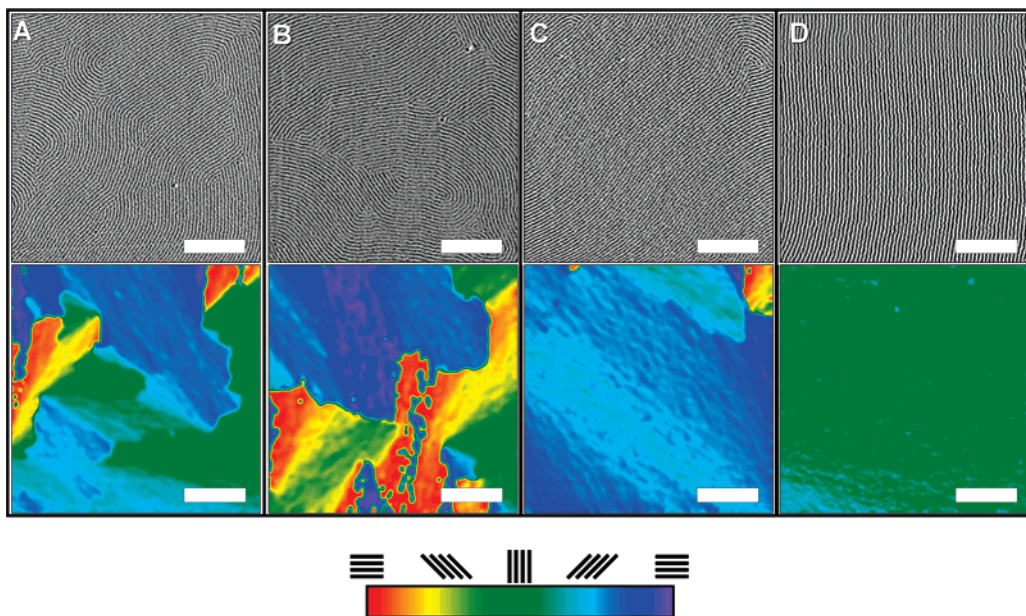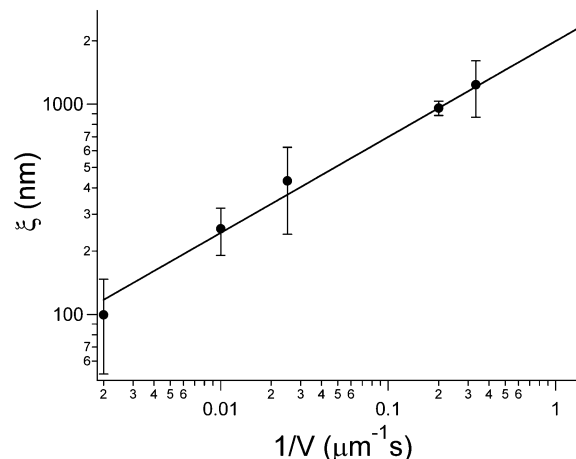
Figure 2. AFM phase images (top) and false color cylinder orientation maps (bottom) of 150 nm PS-PMMA (molar mass = 47 700, f_{ps} = 0.75) films annealed with push velocities of 100 μm/s (A), 40 μm/s (B), 5 μm/s (C), and 1 μm/s (D). The maximum temperature of the sample (T_{Hot}) was ≈ 210 °C with a gradient of ≈ 17 °C/mm. Defect density decreases significantly with decreasing velocity. Sample 1 shows almost no defects within the 2 μm × 2 μm area selected from an actual 5 μm × 5 μm. Differences in cylinder orientation can be visualized using the orientation maps shown on bottom. The color scale indicates the orientation of the cylinders. Scale bars in all images represent 500 nm.
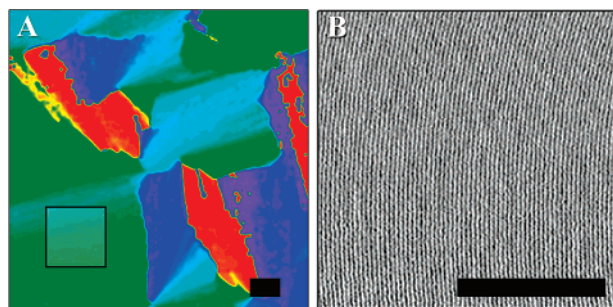
Figure 3. (A) False color cylinder orientation map calculated from a 10 μm × 10 μm AFM phase image of a sample zone annealed at 1 μm/s. (B) Enlarged AFM image detailing the microstructure within the boxed area located in image A showing a high degree of orientational order across the image area. The scale bar in both images is 1 μm.


Figure 4. Correlation length ξ as a function of reciprocal push velocity, V. The fitted line indicates a power law dependence with a fitted exponent of 0.46 ± 0.05 (Uncertainty represents one standard deviation).

PS-PMMA cylinders indicate that $9d$ of annealing at 180 °C is required to achieve grain sizes equal to those obtained by CZA in 90 min.

The coarsening of the grain structure in block copolymer films is usually discussed in terms of a power law relation between ξ and the annealing time, t_{anneal}.[28,31] Our observations can be connected to this type of description by noting that the time over which coarsening actually occurs corresponds to the time regime over which the sample is in a state above the glass-transition temperature, T_g. This "annealing time" varies inversely with V in a CZA measurement because the width of the hot zone is constant for all velocities. In Figure 4, we plot ξ as a function of $1/V$ and find a power law dependence with an exponent of 0.46 ± 0.05.[32] Although the film thickness in our system is greater, our finding can be contrasted against previous observations of an exponent

near $1/4$ for grain coarsening in quasi-two-dimensional monolayer BCP films under isotropic annealing conditions.[28,30,31] General scaling arguments and 2-D simulations based on the Swift−Hohenberg model indicate that the coarsening exponent for isotropic coarsening in block copolymers should equal $1/2$ in the infinite time limit but that smaller *effective exponents* are expected over a wide intermediate time range.[33] Harrison et al. physically interpreted their smaller than expected coarsening exponent value near $1/4$ in isotropic annealing block copolymer measurements to arise from long-range quadrupolar interactions between the defects that inhibit defect coalescence.[28,30] Previous predictions[34] imply that the application of symmetry-breaking

perturbations can give rise to a rapid approach to the long-time scaling limit (exponent equals $^1/_2$), and this prediction has been confirmed by Qian et al.,[33,35] who find an exponent near $^1/_2$ for a system subjected to a simulated ordering field. Our observations are in agreement with these recent theoretical and simulation studies of field-induced ordering kinetics in a model appropriate to describe block copolymer ordering.

Given the large correlation lengths and the apparently different kinetics observed for CZA, the mechanism of coarsening (e.g., defect annihilation) can be expected to differ from traditional thermal annealing of BCPs. It is reasonable to suspect that the differences in observed kinetics between samples that are cold zone annealed vs those that are oven annealed are inherent to the differences in annealing processes. The most obvious difference to consider is thermal history, which has been shown to significantly affect the defect density and order in BCP systems.[16] To determine the role of thermal history in the improved coarsening, a sample was annealed uniformly on a temperature programmable hot stage under nitrogen (static annealing). The stage was programmed to heat the entire sample uniformly with a thermal history equivalent to that of the sample that was cold zone annealed at 1 μm/s. The resulting correlation length for the static annealed sample was an order of magnitude lower ($\xi = 291$ nm) than the CZA sample ($\xi = 2150$ nm), indicating that thermal history is not sufficient to explain the improved coarsening observed during CZA.

Explanations other than thermal history for the increased ordering kinetics can be found by examining the CZA process in more detail. CZA differs from hot zone annealing (HZA) in that ordering develops along a front as the sample first approaches the edge of the hot zone because the BCP material is in the strong segregation limit thermodynamically ($T \ll T_{ODT}$). As the sample moves further into the hot zone, a temperature gradient is established along the sample. This spatiotemporal temperature gradient creates an in-plane spatiotemporal mobility gradient. This effect should be especially large in polymer materials heated from the glassy state because the structural relaxation time in polymer materials normally decreases by over 10 orders of magnitude from T_g to $T_g + 100$ °C (e.g., mobility increases). Recent self-consistent field (SCF) simulations of a moving mobility gradient[36] and Ginzburg–Landau type simulations of a moving quench boundary[37] both indicate that, at slow velocities, well-ordered systems are obtained in which the cylinders locally align during formation with respect to the annealing direction. While not observed by Angelescu et al.[26] in their thin film HZA studies, clear evidence for the predicted alignment was observed experimentally in our measurements. Figure 5 is a plot of the fractional orientation (f_{orient}) or the fraction of the grain map image in which the long axes of the cylinders are oriented within $\pm 30°$ of the zone annealing pushing direction.[38] Alignment of the long axis of the cylinders along the annealing direction becomes more pronounced as V is decreased, which is in qualitative agreement with the aforementioned simulations. Although our experimental resolution is currently limited, we anticipate that the temperature gradient biases the orientation of the
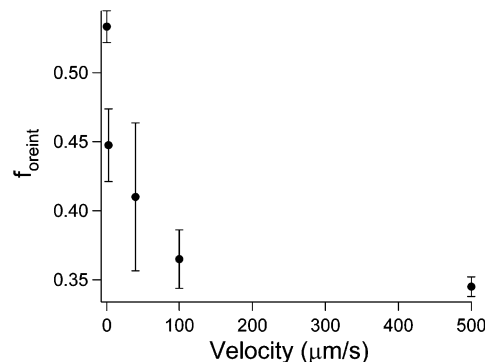
Figure 5. A plot of the fraction of the image oriented such that the long axis of the cylinder is aligned within $\pm 30°$ of the annealing direction (f_{orient}). Consistent with simulations,[34,35] the degree of alignment of the long-axis of the cylinder with annealing direction increases dramatically as the annealing velocity is decreased.
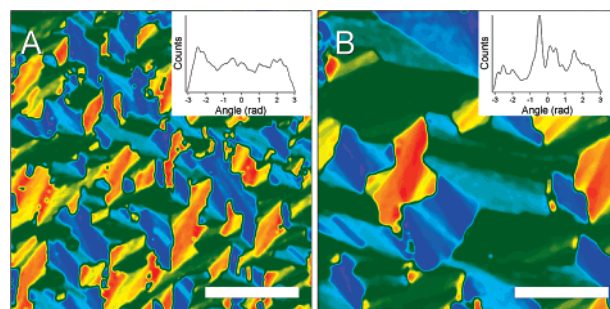
Figure 6. (A) False color director angle images of a sample oven annealed at 180 °C for 18 h. This produces a correlation length of $\xi = 247$ nm and a fraction of the image oriented within $\pm 30°$ of the annealing direction (f_{orient}) of 0.33. (B) False color cylinder orientation map following cold zone annealing at 1 μm /s ($T_{Hot} = 210$ °C, $G = 17$ °C/mm) of the oven annealed sample in (A), indicating an increases in ξ to 570 nm, and an increase in f_{orient} to 0.49. The histograms (insets) of the images show a clear increase in the number of cylinders oriented with the annealing direction (0 rad), suggesting that during CZA, cylinders tend to reorient with the annealing direction.

grains *as they form*, which in turn strongly influences the subsequent evolution and defect annihilation. This interpretation is consistent with the mechanism of the enhanced defect annihilation that occurs as a result of preferential alignment of BCPs in applied electric fields.[7,8,39−43]

The results presented in Figure 2 demonstrate the effects of CZA on "as-cast" films, without significant pre-existing grains; however, its effect on misaligned cylinders is also of interest. To study the effect of the moving temperature gradient on randomly oriented cylinders, a sample was oven annealed under vacuum at a constant temperature (180 °C) for 18 h and then quenched and analyzed. The sample was then subsequently cold zone annealed at 1 μm/s ($T_{Hot} = 210$ °C, $G = 17$ °C/ mm). Figure 6 contains 5 μm × 5 μm cylinder orientation maps of the traditionally annealed sample at 180 °C (A) and the same sample after it was subsequently cold zone annealed (B). The correlation lengths of the two samples were determined to be 247 and 570 nm, respectively. The increase in ξ is significantly larger than what would be expected from subjecting the sample instead to further constant temperature oven annealing, providing evidence for

an increase in the extent of defect annihilation. Analysis of the distribution of cylinder orientations provides more insight into the mechanism of this improved coarsening. The histograms of images A and B (insets) show a significant increase in the number of cylinders oriented with the annealing direction, from $f_{orient} = 0.33$ (expected value for randomly oriented cylinders) after oven annealing to $f_{orient} = 0.49$ following cold zone annealing. This result suggests that the temperature gradient results in progressive local reorientation of misoriented cylinders, which can also facilitate defect annihilation.

Although the increased order observed in Figure 6 suggests that the temperature gradient enhances defect annihilation, the final correlation length ($\xi = 570$ nm) is far less than that of the sample that was cold zone annealed from the as-cast film ($\xi = 2150$ nm). This situation is similar to the findings by Böker et al.,[43] who found it was difficult to realign BCP polymer materials with electric fields once a low-energy, highly ordered state orthogonal to the field direction had been formed. Although ξ of the oven annealed sample is relatively low, recent simulation studies and analytic theory have indicated that block copolymers under isotropic annealing conditions evolve into low-energy metastable configurations that are highly persistent.[44,45] As a result of the energetically frustrated nature of the oven annealed sample, reorientation of the randomly oriented cylinders is difficult. It is therefore reasonable to assume that the large correlation lengths obtained via CZA are the result of both the orientational bias present during grain formation as well as the enhanced defect annihilation facilitated by the reorientation of initially misaligned cylinders.

In summary, cold zone annealing has been shown to be an effective means of controlling defects in block copolymer thin films. This technique is particularly attractive because it does not require annealing above the T_{ODT}, which is inaccessible for some block copolymer materials. CZA is also an effective tool for studying the development of order under an applied temperature gradient. The kinetics of ordering for asymmetric PS-PMMA are much faster than traditional thermal annealing, resulting in $5-30$ μm^2 area grains in less than 5 h. This enhancement in coarsening kinetics is likely due to enhanced defect annihilation facilitated by preferential alignment of the BCP cylinders in the temperature gradient. While the grain size produced is still an order of magnitude less than that needed for many applications, one can imagine that combining this technique with top-down techniques such as graphoepitaxy might lead to an industrially accessible approach to achieving well-ordered BCP morphologies over very large areas in short times. In addition, the preferential alignment with the annealing direction provides unprecedented control over cylinder alignment using existing thermal annealing techniques alone. This ability to control the alignment of the morphology coupled with the ability to control orientational order makes CZA a useful platform with which to probe the evolution of long-range order in technologically important block copolymer materials.

References

(1) Hawker, C. J.; Russell, T. P. *MRS Bull.* **2005**, *30*, 952−966.
(2) Stoykovich, M. P.; Nealey, P. F. *Mater. Today* **2006**, *9* (9), 20−29.
(3) Li, M. Q.; Ober, C. K. *Mater. Today* **2006**, *9* (9), 30−39.
(4) Segalman, R. A. *Mater. Sci. Eng., R* **2005**, *48*, 191−226.
(5) Kim, S. H.; Misner, M. J.; Russell, T. P. *Adv. Mater.* **2004**, *16*, 2119.
(6) Kimura, M.; Misner, M. J.; Xu, T.; Kim, S. H.; Russell, T. P. *Langmuir* **2003**, *19*, 9910−9913.
(7) Amundson, K.; Helfand, E.; Quan, X.; Smith, S. D. *Macromolecules* **1993**, *26*, 2698−2703.
(8) Amundson, K.; Helfand, E.; Quan, X. N.; Hudson, S. D.; Smith, S. D. *Macromolecules* **1994**, *27*, 6559−6570.
(9) Mansky, P.; DeRouchey, J.; Russell, T. P.; Mays, J.; Pitsikalis, M.; Morkved, T.; Jaeger, H. *Macromolecules* **1998**, *31*, 4399−4401.
(10) Morkved, T. L.; Lu, M.; Urbas, A. M.; Ehrichs, E. E.; Jaeger, H. M.; Mansky, P.; Russell, T. P. *Science* **1996**, *273*, 931−933.
(11) Thurn-Albrecht, T.; DeRouchey, J.; Russell, T. P.; Jaeger, H. M. *Macromolecules* **2000**, *33*, 3250−3253.
(12) Xu, T.; Zhu, Y. Q.; Gido, S. P.; Russell, T. P. *Macromolecules* **2004**, *37*, 2625−2629.
(13) Xu, T.; Zvelindovsky, A. V.; Sevink, G. J. A.; Lyakhova, K. S.; Jinnai, H.; Russell, T. P. *Macromolecules* **2005**, *38*, 10788−10798.
(14) Sundrani, D.; Darling, S. B.; Sibener, S. J. *Langmuir* **2004**, *20*, 5091−5099.
(15) Sundrani, D.; Darling, S. B.; Sibener, S. J. *Nano Lett.* **2004**, *4*, 273−276.
(16) Hammond, M. R.; Cochran, E.; Fredrickson, G. H.; Kramer, E. J. *Macromolecules* **2005**, *38*, 6575−6585.
(17) Segalman, R. A.; Hexemer, A.; Kramer, E. J. *Macromolecules* **2003**, *36*, 6831−6839.
(18) Kim, S. O.; Solak, H. H.; Stoykovich, M. P.; Ferrier, N. J.; De Pablo, J. J.; Nealey, P. F. *Nature* **2003**, *424*, 411−414.
(19) Stoykovich, M. P.; Muller, M.; Kim, S. O.; Solak, H. H.; Edwards, E. W.; de Pablo, J. J.; Nealey, P. F. *Science* **2005**, *308*, 1442−1446.
(20) Bechhoefer, J.; Libchaber, A. *Phys. Rev. B: Condens. Matter Mater. Phys.* **1987**, *35*, 1393−1396.
(21) Stefanescu, D. M.; Moitra, A.; Kacar, A. S.; Dhindaw, B. K. *Metall. Mater. Trans. A* **1990**, *21*, 231−239.
(22) Misbah, C.; Valance, A. *Phys. Rev. E* **1995**, *51*, 1282−1290.
(23) Bodycomb, J.; Funaki, Y.; Kimishima, K.; Hashimoto, T. *Macromolecules* **1999**, *32*, 2075−2077.
(24) Hashimoto, T.; Bodycomb, J.; Funaki, Y.; Kimishima, K. *Macromolecules* **1999**, *32*, 952−954.
(25) Mita, K.; Tanaka, H.; Saijo, K.; Mikihito, T.; Hashimoto, T. *Macromolecules* **2007**, *40*, 5923.
(26) Angelescu, D. E.; Waller, J.; Adamson, D. H.; Register, R. A.; Chaikin, P. M. *Adv. Mater.* **2007**, in press.
(27) Certain equipment, instruments, or materials are identified in this paper in order to adequately specify the experimental details. Such identification does not imply recommendation by the National Institute of Standards and Technology nor does it imply the materials are necessarily the best available for the purpose.
(28) Harrison, C.; Adamson, D. H.; Cheng, Z. D.; Sebastian, J. M.; Sethuraman, S.; Huse, D. A.; Register, R. A.; Chaikin, P. M. *Science* **2000**, *290*, 1558−1560.
(29) Harrison, C. Ph.D. Thesis. Princeton University, Princeton, NJ, 1999.
(30) Harrison, C.; Cheng, Z. D.; Sethuraman, S.; Huse, D. A.; Chaikin, P. M.; Vega, D. A.; Sebastian, J. M.; Register, R. A.; Adamson, D. H. *Phys. Rev. E* **2002**, *66*, 011706.
(31) Black, C. T.; Guarini, K. W. *J. Polym. Sci., Part A: Polym. Chem.* **2004**, *42*, 1970−1975.
(32) The data in this manuscript in the figures and in the tables are presented along with the standard uncertainty involved in the measurement, where the uncertainty represents one standard deviation from the mean.
(33) Qian, H.; Mazenko, G. F. *Phys. Rev. E* **2003**, *67* (3).
(34) Pismen, L. M. *Vortices in Nonlinear Fields;* Oxford University Press: London, 1999.
(35) Qian, H.; Mazenko, G. F. *Phys. Rev. E* **2006**, *73*, 036117.
(36) Bosse, A. W.; Douglas, J. F.; Berry, B. C.; Jones, R. L.; Karim, A. manuscript in preparation.

(37) Zhang, H. D.; Zhang, J. W.; Yang, Y. L.; Zhou, X. D. *J. Chem. Phys.* **1997**, *106*, 784−792.

(38) As a result of small uncertainties associated with the exact spatial correlation of the acquired image and the annealing direction, a rather large angle range was chosen for the calculation of the fraction of the cylinders oriented with the annealing direction.

(39) Boker, A.; Elbs, H.; Hansel, H.; Knoll, A.; Ludwigs, S.; Zettl, H.; Urban, V.; Abetz, V.; Muller, A. H. E.; Krausch, G. *Phys. Rev. Lett.* **2002**, *89*, 135502.

(40) Ludwigs, S.; Schmidt, K.; Stafford, C. M.; Amis, E. J.; Fasolka, M. J.; Karim, A.; Magerle, R.; Krausch, G. *Macromolecules* **2005**, *38*, 1850−1858.

(41) Olszowka, V.; Hund, M.; Kuntermann, V.; Scherdel, S.; Tsarkova, L.; Boker, A.; Krausch, G. *Soft Matter* **2006**, *2*, 1089−1094.

(42) Schmidt, K.; Schoberth, H. G.; Schubert, F.; Hansel, H.; Fischer, F.; Weiss, T. M.; Sevink, G. J. A.; Zvelindovsky, A. V.; Boker, A.; Krausch, G. *Soft Matter* **2007**, *3*, 448−453.

(43) Schmidt, K.; Boker, A.; Zettl, H.; Schubert, F.; Hansel, H.; Fischer, F.; Weiss, T. M.; Abetz, V.; Zvelindovsky, A. V.; Sevink, G. J. A.; Krausch, G. *Langmuir* **2005**, *21*, 11974−11980.

(44) Boyer, D.; Vinals, J. *Phys. Rev. E* **2002**, *65*, 046119.

(45) Zhang, C. Z.; Wang, Z. G. *Phys. Rev. E* **2006**, *73*, 031804.

NL071354S